

## WAVE PROPAGATION IN SOFT SOLID HALF SPACES AND EVANESCENT PRESSURES IN OVERLYING WATER

Richard (Dick) Hazelwood, Patrick Macey

R&V Hazelwood Associates LLP, Guildford GU2 8UT, UK  
PACSYS Ltd, Strelley Hall, Nottingham, NG8 6PE, UK

Dr R A Hazelwood, 14 Ash Grove, Guildford GU2 8UT, UK, [dick@r-vhazelwood.co.uk](mailto:dick@r-vhazelwood.co.uk),  
[aconic@zen.co.uk](mailto:aconic@zen.co.uk)

### **Abstract:**

*Typical sedimentary seabeds have very slow shear wave speeds which increase with depth. This can be modeled with a linear depth profile of the shear wave speed. A simpler model has uniform solid material under a fluid half space, both extending to infinity as described by Scholte. Finite element modeling has been used to study both, when the solid is deformed by an impact, simulating piling or dredging actions. Off shore piling is used for wind turbine installation, and the consequences to seabed wildlife are associated with the wave energy which is radiated outward.*

*In addition to the ground roll interface waves, as discussed at earlier conferences, we find other wave forms which may also contribute to the vibrations in seabed sediments and the evanescent pressures they create in adjacent water. Wave propagation in the linear graded solid model can be predicted using circular ray pathways, all of which have their centre at the same height above the seabed. This is controlled by the shear speed profile.*

**Keywords:** *Seismic interface waves, Half space model, Water particle velocity, piling, dredging*

**1. INTRODUCTION**

Previous studies showed how the propagation of seismic interface waves depends on the nature of the seabed [1],[2]. They led to the modelling of a saturated sedimentary seabed by a modified infinite half space. Rayleigh [3] described a simple half space of a uniform solid under a vacuum and Scholte [4] showed that similar interface waves would be seen when the upper half space was a fluid.

A more realistic model uses a graded solid, where the material shear wave speed increases linearly with depth. This model supports a special wavelet which propagates well if suitably excited. This is described as a Morphing Mexican Hat (MMH) form. It is efficiently excited by the Ricker form (a.k.a. Mexican Hat), of a suitable period, to repeatedly morph via a hump to a dip (inverted), and back, without dissipating energy into a longer period. In contrast we discuss the consequence of using a wavelet with a shorter period, which then expands in time, with a greater loss of peak intensity than predicted by cylindrical spreading.

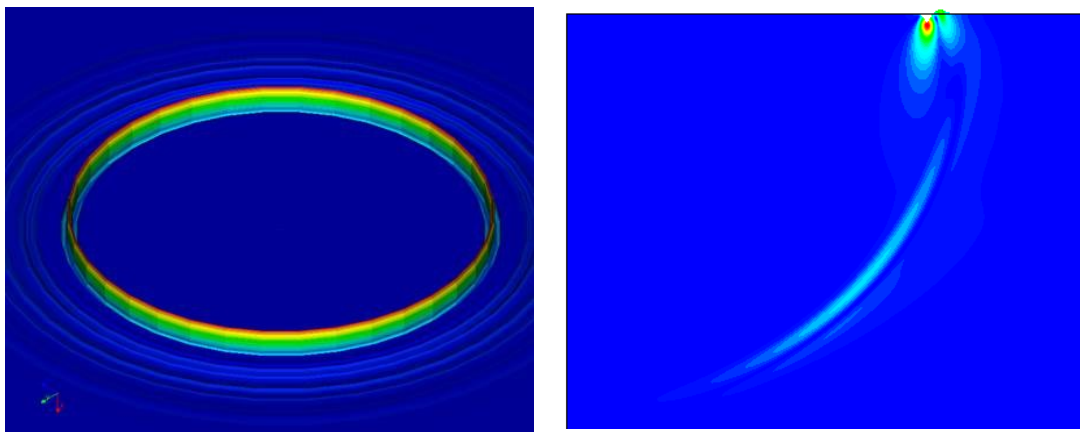


*Fig 1: Two views of a seismic wavelet in an axisymmetric model. In the view from above, the axis of symmetry is central, whereas it is on the left in the cross section, showing the energy radiating from the interface into the depths for a Scholte model with uniform solid material. Whilst the most intense vibration occurs at the surface, a shear wave arc propagates into the depths. The vibration amplitude is colour coded, and the deformation exaggerated for clarity. After 1.25s, the interface wave in the 2<sup>nd</sup> view has reached a radius of almost 150m.*

The axisymmetry assumed in these finite element (FE) models allows results to be presented as a cross section in two dimensions (2D), and then enlarged to show details.

**2. THE SIMULATION OF THE IMPACT AND THE AIRY PHASE**

The earlier work on pile driving represented the piling impact as a force on the substrate around a circular pile base, shown as a point on the 2D view, radius RP, in the FE model.

Model	RP= 0m	RP= 0.5m	RP= 1m	RP= 2m	RP= 4m
Energy	680J	657J	593J	409J	161J

*Table 1: The energy accepted by the solid as a function of radius for the excitation*

However, wavelet forms as seen in the far field showed little dependency on the radius of the node to which the vertical force was applied. A confirmatory study showed how the energy accepted by the solid, as this radius was decreased, showed a limit case at radius zero.

This simplification then allowed attention to be placed on the time profile of the applied force. Shearer [5] stated that seismologists often use the Ricker wavelet in their simulations

$$R_k(T) = K e^{-\frac{T^2}{2}} (1 - T^2) \quad \text{where } T = \frac{2(t - t_0)}{\tau} \quad (1)$$

Here the time has been scaled by the use of a pulse width  $\tau$ , about a centre maximum at time  $t_0$ . The central peak lies between two zeroes, occurring when  $T^2 = 1$  or  $t - t_0 = \pm \tau/2$ . This shape is often called the Mexican Hat. The peak force  $K$  was always set to 1MN.

The zero/zero time  $\tau$ , or pulse width, then governs the frequency spectrum of the energy of excitation. This can affect the speed of the interface wave in the graded model. Half space models with a uniform solid show no such effect, and are thus unrealistic, whereas many more realistic assumptions provide dramatic dispersion of input waves.

In earlier work a more realistic model used data on shear wave speed profiles with depth, taken from reviews by Hamilton [6] of measured values from various seabed types. Later it was found that a linear gradient of material shear speeds yielded a MMH wavelet, which propagated with little loss. By using a Ricker excitation, the interface wave was seen to morph from a hump to a dip and back at a rate determined by the shear speed profile.

The modelling ignored any absorption, but gave a good fit to a cylindrical energy spreading rule, with successive hump forms correlating well in their shape. This gave precise values for the group velocity, between two symmetric humps, smaller than the value of the shear wave speed as set in the model (often 128m/s). However, for these material values, there was a clear minimum seen when the width  $\tau$  of the excitation was around 35ms.

	Pulse width $\tau$ ms	Transit speed $\text{ms}^{-1}$	Hump #1 width ms	Hump #2 width ms
1	16	117.89	15.4	16.6
2	20	117.74	18.8	20.4
3	25	117.5	23	24
4	32	117.38	29	29
5	40	117.39	36	36
6	50	117.60	45	45
7	64	117.92	56.3	58
8	80	118.79	70.4	74
9	100	119.47	86	88

Table 2. Wavelet properties taken from runs with different Ricker drive pulse widths.

The investigation of the shorter pulses was limited by the break-up of the resultant wavelets with distance, as dispersion caused them to be spread in time. An improved model has allowed the pulse widths to be further reduced, whilst still allowing sufficient correlation to better determine the group speed.

Note that the width (zero/zero times) of successive symmetric hump forms increases with time and distance when well away from the minimum in transit speed. At the minimum speed this wavelet expansion was also minimised.

This minimum is an example of what Shearer [5] describes as an Airy phase. Earth's geology is also layered, but on a much larger scale, leading to stable propagation of a variety of earthquake forms, including the interface wave (Rayleigh wave) with its strong horizontal motion, so destructive to buildings. Note the time scale is in minutes not milliseconds.

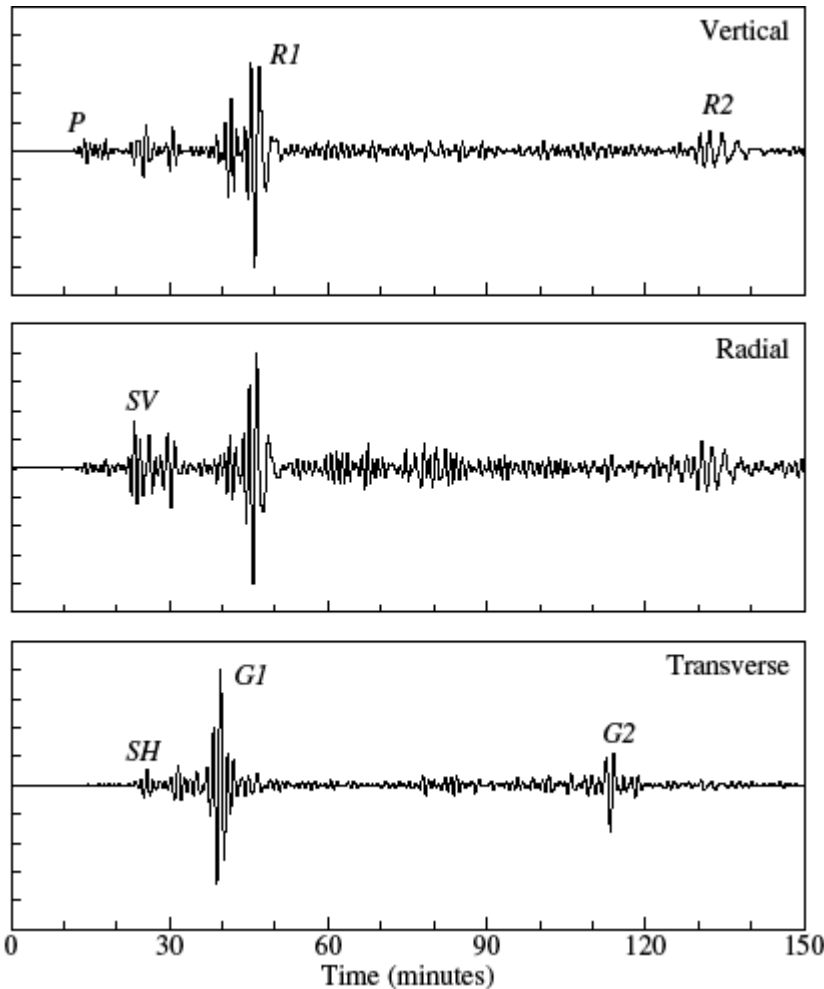


Fig 2: An example of a powerful earthquake as recorded after propagation across the Pacific ocean in 1989. Taken from Shearer [5] with permission. Waves include dominant Rayleigh (R1,R2) types as well as shear (SV and SH) and Love waves (G1,G2).

### 3. RESULTS FROM A MORE DETAILED FE MODEL

The mathematical model which gives a stably propagating, but morphing MMH compact form has a smooth linear increase in material stiffness with depth,  $d$ , as set by the shear wave speed function,  $V_s(d)$ . This is set by the interface value ( $d=0$ ) and the gradient with depth,  $g$ . The gradient has been shown to control the morphing rate

Shear speed gradient ( $s^{-1}$ )	1	2	4	8	16	32
Morphing frequency (Hz)	0.335	0.748	1.488	2.912	5.682	10.91

Table 3: The variation of the morphing frequency with the shear wave speed gradient.

A gradient of 4 (m/s)/m (also shown as  $s^{-1}$ ) was often convenient, and a fairly good fit to the measured data reported by Hamilton [6]. The regular morphing occurs at 1.488Hz for this gradient. These MMH wavelets are an extreme example of the way wave groups are seen to progress with their peaks moving through the group envelope due to the difference between group velocity and phase velocity.

The finite elements of the FE model have material properties set in layers, but each successive layer of elements has its own different property. Recent models use 56 different values to better approximate the smooth curve of the physical model

#### 4. RAYS IN A LINEAR GRADIENT FOLLOW ARCS OF CIRCLES

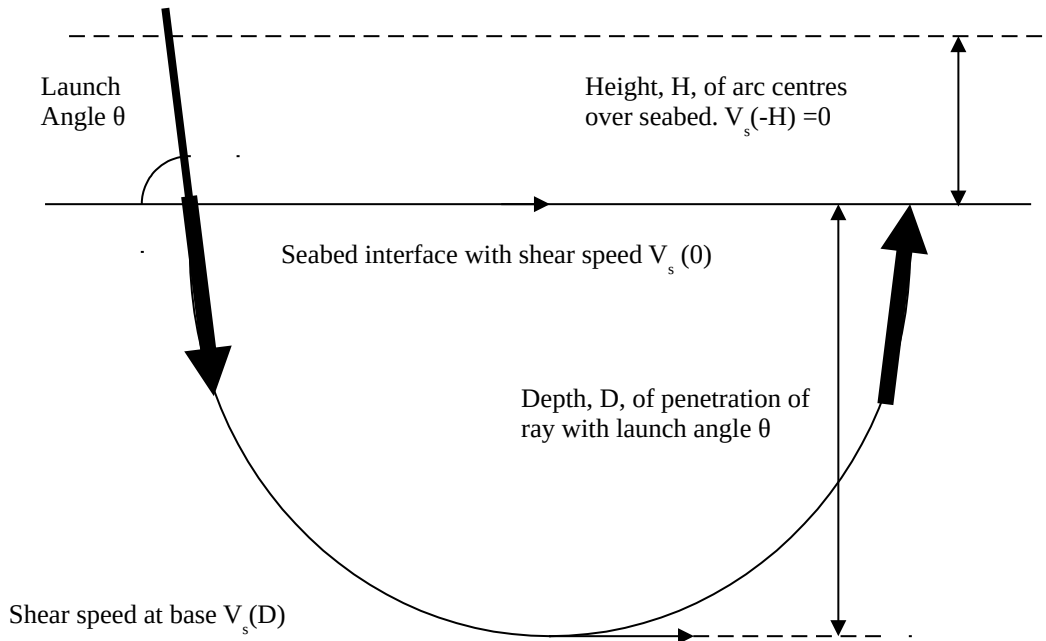


Fig 3: Rays (and corresponding plane waves) being refracted back to the interface

Plane pressure waves in water are well known to suffer refraction. Their paths can be analysed by ray tracing in most circumstances. Shearer [5] discussed the use of ray tracing for plane shear waves in solids. Whereas the shear waves in a Scholte model (Fig 1) pass down into the depths, they will be refracted by a shear speed depth gradient, just as sound pressure waves are refracted by the gradient of sound speed in water. Kinsler et al [7] showed that for a mixed layer, the refraction due to increasing pressure with depth gives ray paths as arcs of circles.

Snell's law leads to a constant "horizontal slowness" dependent on the launch angle  $\theta$  (Shearer). This ray constant then controls the arc paths as shown in Fig 3. All ray paths are centred at the same height  $H$  above the interface, which is the height at which the shear speed function  $V_s(d)$  becomes zero if extrapolated.  $D$  is the maximum depth for each ray which depends on  $\theta$ . The travel time for the return to the interface ( $d=0$ ) will also depend on  $\theta$ .

#### 5. A SHORTER WAVELET IS DISPERSED IN A GRADED MEDIUM

Whilst earlier studies concentrated on the properties of the compact MMH wavelet, seen at the Airy phase around periods  $\sim 35$ ms, dispersion occurs for pulses with different frequency contents. A Ricker wave of width  $\tau = 8$ ms is shown to have expanded to give many zero crossing times in plots of vibration displacement. This model "fg5w" uses 56 different material properties for the finely graded interface elements, as seen in Fig 4. Data is computed for every successive 0.4ms step in the 3.2 second long transient analysis. The smallest solid elements are 0.25m deep by 0.2m radially, much finer than those used earlier, to allow the pulse width to be reduced. Poisson's ratio for the solid starts close to 0.5 but tends to 0.25 at infinity. The solid density is 2250 kg/m<sup>3</sup>, and its pressure wave speed is 1520m/s at the interface. Water pressure speed is 1500m/s, and water density is set at 1000kg/m<sup>3</sup>.

The detailed view in Fig 4, of the state at 1.6s, after 4000 steps, only shows 5m depth of overlying water and 7m depth of sedimentary seabed. The gap between them is for clarity.

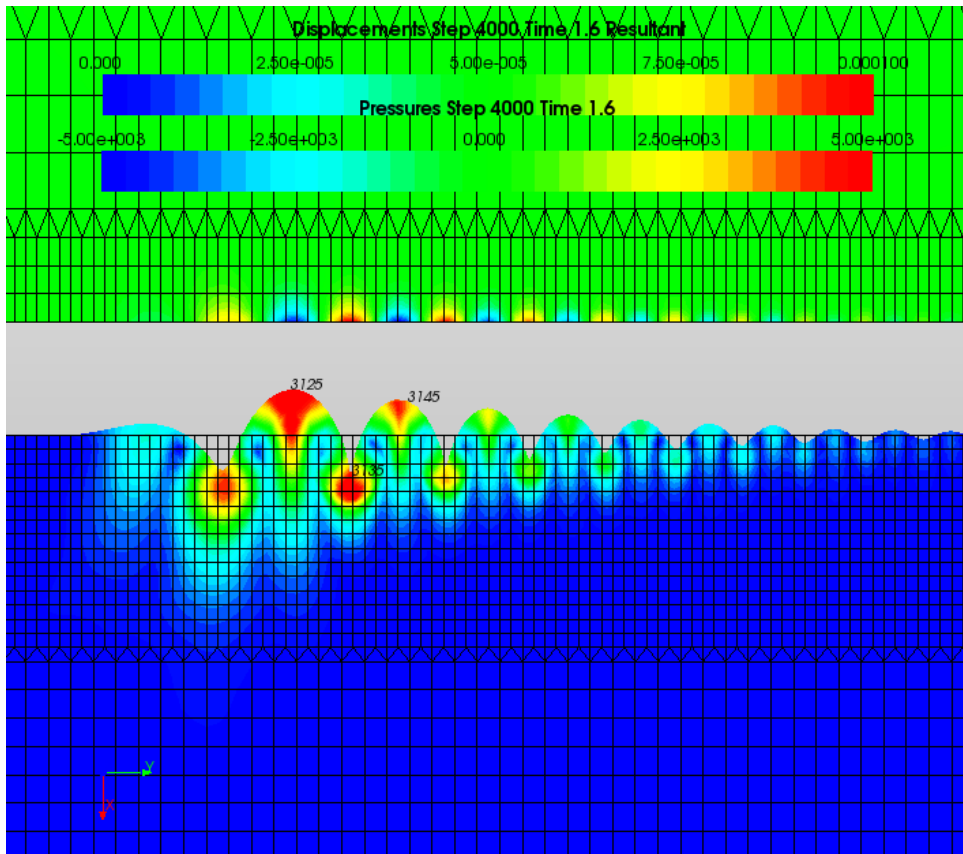


Fig 4: The displacement in the solid and pressures in the overlying water. Deformations are exaggerated. Peak pressures exceed 500Pa, and displacements exceed 100 $\mu$ m

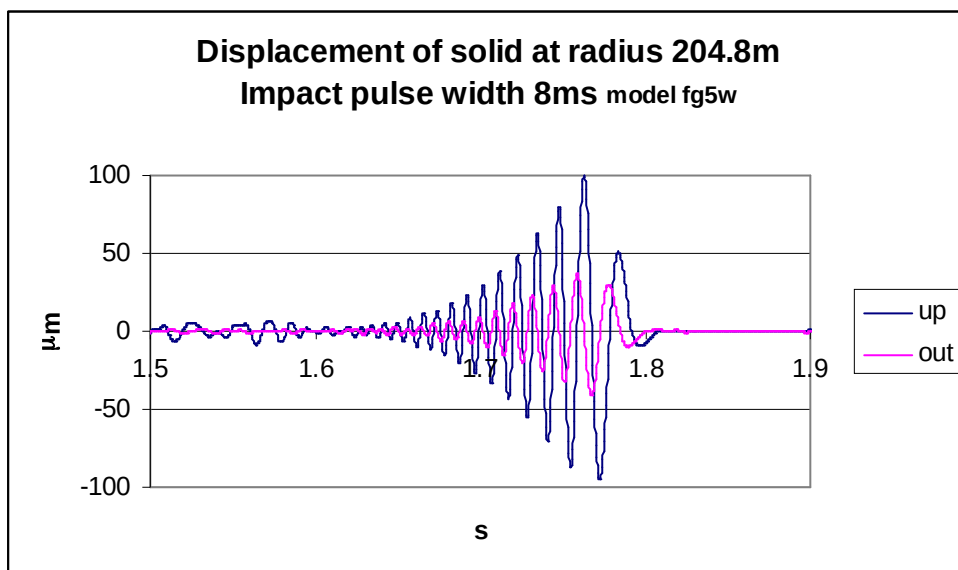


Fig 5: Despite having expanded in time to show many zero crossings, the upward displacement remains out of phase with the radial outward displacement. This retrograde ellipsoidal motion has a maximum inward velocity as upward displacement peaks.

## 6. THE EVANESCENT PRESSURES CLOSE TO THE SEABED

The acoustic pressures in the water close to the seabed rapidly reduce as heights increase

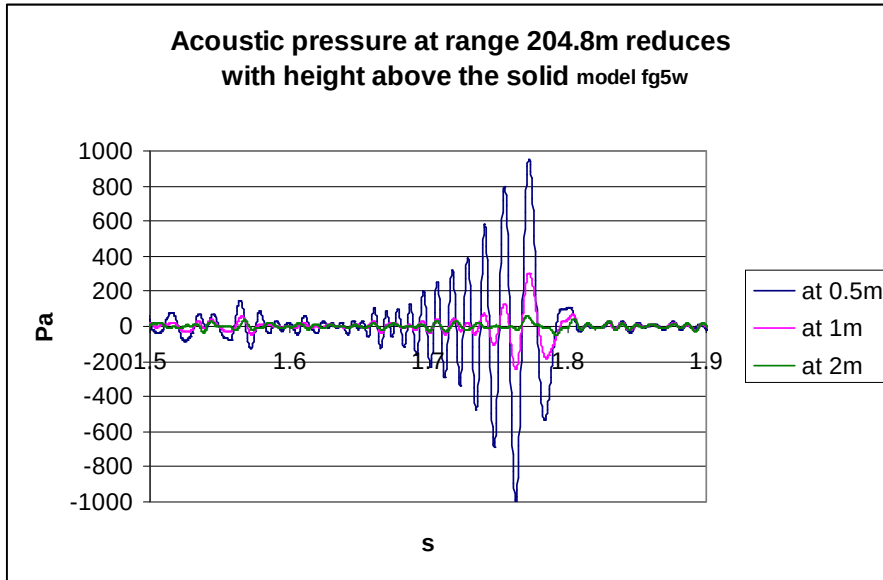


Fig 6: The acoustic pressures predicted by model run fg5w at three different heights

The pressure measured by hydrophone can be used to assess the solid motion

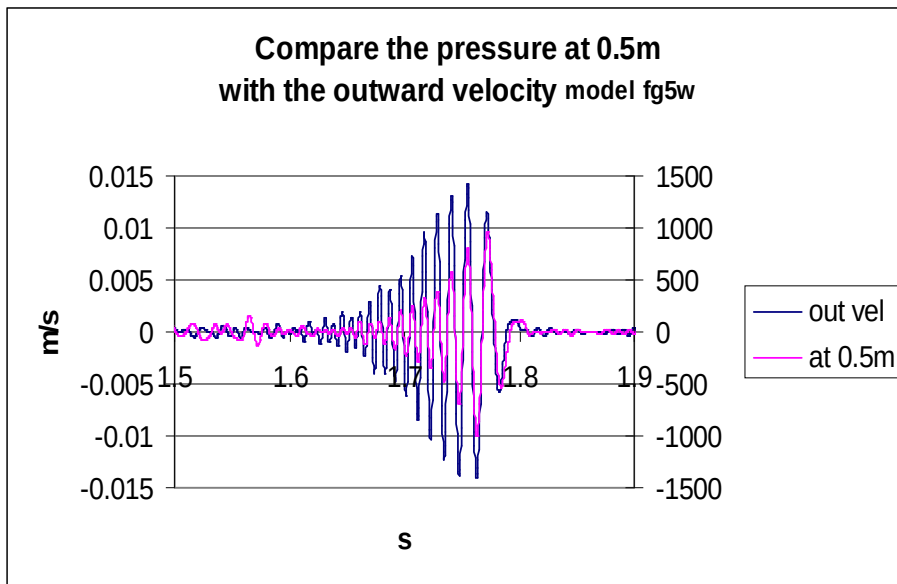


Fig 7: There is a good match between the times of zero crossings for predicted water pressures (right axis) and the outward velocity of the solid beneath (left axis).

The peak evanescent acoustic pressure  $p_E = -999\text{Pa}$  (mauve) corresponds to  $u_h = -13.7\text{ mm/s}$  outward velocity of the solid (largest negative peaks). The ratio is  $72920\text{ Pa/(m/s)}$ . This has the units of an impedance and can be compared to a typical specific acoustic impedance in seawater of  $1.5\text{ MPa/(m/s)}$ . As the hydrophone is raised, this  $p_E/u_h$  ratio will be reduced.

Strong seabed motion may thus be sensed by the detection of these evanescent pressure measurements, whose characteristics should allow them to be distinguished from other pressure waves. The times of the evanescent zero crossings are independent of the height above the seabed.

## 7. LINKING WATER PARTICLE VELOCITIES TO ACOUSTIC PRESSURE

The motion of the water near the seabed mimics that of the solid, but with larger horizontal motion. Vertical motions must be the same at the interface, but decay with height above it. However, the constraint on horizontal motion of the solid, as seen by the typical ellipsoidal paths is not present for the fluid, giving a substantial amplification of this key parameter.

Horizontal water particle velocities,  $u_h$ , for the MMH wavelet were modelled, and found to closely mimic the evanescent acoustic pressures,  $p_E$ , at the same point, given little or no dispersion. Theory then gives this ratio as proportional to the evanescent wavelet speeds,  $V_E$ , and the density of the water,  $\rho$ . This ratio does not change with height over the seabed

$$\frac{p_E}{u_h} = \rho V_E \quad (2)$$

Note the similarity to the relation for a bulk pressure wave. A measured evanescent acoustic pressure thus predicts a much larger water particle velocity than that indicated for the same value bulk pressure wave, by a typical factor of the ratio of wave speeds 1500/117.4, more than a factor 12 larger. Some experimental confirmation has been achieved.

Current work involves further investigation of this link, hoping to be able to detect and measure the presence of ground roll vibrations using the more convenient deployment of a seabed mounted hydrophone array. Ideally this should be done in conjunction with the seabed geophone sledge.

## 8. ACKNOWLEDGEMENTS

The authors are grateful to Peter Shearer for permission to use his figure

## REFERENCES

1. **Hazelwood, R.A. Macey, P.C.** Modelling water motion near seismic waves propagating across a graded seabed, as generated by man-made impacts. *J. Mar. Sci. Eng.*, 4(3), 47, 2016
2. **Hazelwood, R.A. Macey, P.C. Robinson S.P. Wang L. S.** Optimal transmission of interface vibration wavelets- a simulation of seabed responses. *J. Mar. Sci. Eng.*, 6, 61, 2018
3. **Rayleigh, L.** Interface waves. *Proc. Lond. Math. Soc.*, 17, 4–11, 1887.
4. **Scholte, J.G.** On true and pseudo Rayleigh waves. *Proc. K. Ned. Akad. Wet. Amst.*, 52, 652–653, 1949.
5. **Shearer, P.M.** *Introduction to Seismology*; Cambridge University Press: Cambridge, UK, 1999
6. **Hamilton, E.L.**  $V_p/V_s$  and Poisson's ratio in marine sediments and rocks. *J. Acoust. Soc. Am.*, 66, 1093–1101, 1979.
7. **Kinsler L.E. Frey A.R. Coppens A.B. Sanders J.V.** *Fundamentals of Acoustics* 3<sup>rd</sup> Ed, John Wiley & Sons, New York, 1980